analytical chemistry

pubs.acs.org/ac Article

Size-Dependent Deformation and Competition H-Bond Site-Induced Individual Fluorescence Response of a Single-Crystal Three-Dimensional Covalent Organic Framework

Yan Wang, Xu-Qin Ran, Cheng Yang, Hai-Long Qian,* and Xiu-Ping Yan

Cite This: https://doi.org/10.1021/acs.analchem.4c00217 Read Online

ACCESS | Metrics & More | Article Recommendations | Supporting Information

ABSTRACT: Understanding the individual fluorescence response mechanism of covalent organic frameworks (COFs) at a single-crystal level is of great significance for the rational design of COF-based microsensors but unreachable because all previous COF-based sensors are performed with average fluorescence response behavior of various sized polycrystalline COFs. Herein, we design to explore the fluorescence response of a monodisperse single-crystal COF and further reveal the individual heterogeneity of the response mechanism. Three-dimensional single-crystal COF-301 (SCOF-301) with an intramolecular H-bond-induced excited-state intramolecular proton-transfer effect is selected as a proof-of-concept SCOF. With ethanol, benzene, and ammonia as model analytes, three different deformation and competition H-bond site-induced fluorescence response mechanisms related to crystal size are revealed. Small single particles of SCOF-301 (SSCOF-301) exhibit a more flexible structure, leading to the dominant role of deformation in the fluorescence response of small-sized SSCOF-301. The decreasing flexibility of SSCOF-301 with the increase of crystal size results in involvement of competition of the H-bond site to the fluorescence response besides deformation. Further increase of the crystal size makes the large-sized SSCOF-301 difficult to deform; thus, the competition of the H-bond site dominates the fluorescence response. This work provides a deep understanding of the individual fluorescence response mechanism of COFs to guide the design of a functional COF sensor with suitable size and mechanism for different structural analytes.

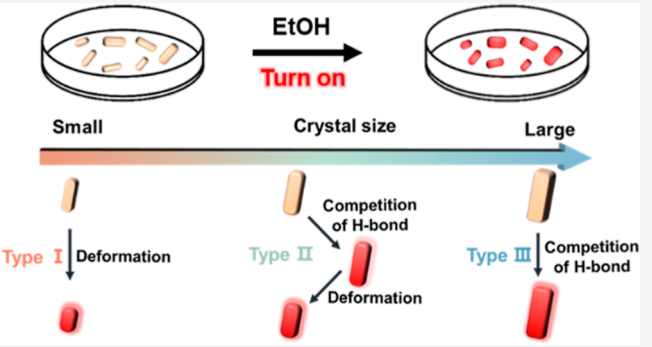

Covalent organic frameworks (COFs) are porous crystalline polymers with a predesignable π-conjugated structure at the atomic level.[1,2] The ordered structure of COFs with extended π-conjugation is conducive to the transport of charges, effectively amplifying the fluorescent signal.[3−5] In addition, the predesignability and tunability allow precise introduction of functional units into COFs to promote the specificity to targets.[6,7] These excellent properties imply the great potential of COFs as fluorescent materials for sensing. So far, COFs have attracted extensive attention in fluorescence sensing of explosives,[8,9] heavy metals,[10] biomolecules,[11] and volatile organic compounds.[12]

Dynamic covalent chemistry is the foundation of COFs.[13,14] The reversible covalent bond allows error correction during the condensation of monomers to promote the formation of crystalline networks.[15,16] However, high polymerization speed of monomers and inherently weak reversibility of covalent bond make the nucleation and error correction difficult to control, leading to easy formation of irregular polycrystalline COFs (PCOFs) with a wide range of sizes, whose crystals consist of different orientations of planes.[17,18] Thus, the fluorescent signal of COF sensors is mainly based on the average data of PCOF powders,[19−22] while the effect of individual heterogeneity on the fluorescence response is impossible to evaluate.

In 2018, single-crystal COFs (SCOFs) were successfully synthesized for the first time via addition of a competitive inhibitor to control the nucleation rate.[19] As a whole crystal is composed of a continuous lattice, SCOFs always appear in uniform and monodisperse micron-scale size and exhibit higher crystallinity than PCOFs.[23−28] The superiority in morphology and crystallinity makes SCOFs more promising than PCOFs in chromatography,[29] adsorption,[30] and thermal conductivity.[31] More importantly, uniform monodisperse SCOFs make it possible to study the fluorescence sensing performance of COFs at the single-crystal level so that the fluorescence

Received: January 11, 2024
Revised: February 25, 2024
Accepted: March 19, 2024

https://doi.org/10.1021/acs.analchem.4c00217
Anal. Chem. XXXX, XXX, XXX−XXX

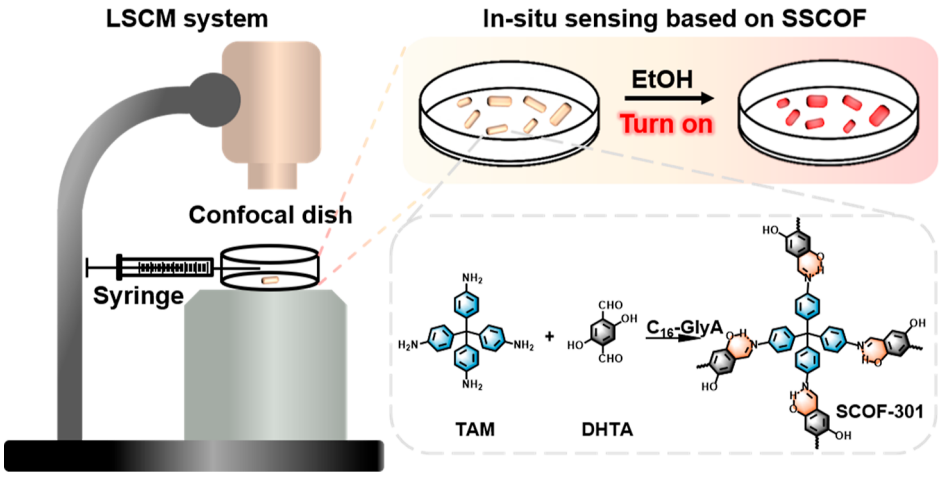

Figure 1. In situ fluorescence response of monodisperse SSCOF-301 to EtOH recorded with the LSCM system.

response mechanism of individual crystal COFs can be further explored.

Herein, we design to explore the fluorescence response of a monodisperse SCOF and further reveal the individual heterogeneity of response mechanism. As a proof of concept, fluorescent three-dimensional single-crystal COF-301 (SCOF-301) with an intramolecular H-bond-induced excited-state intramolecular proton transfer (ESIPT) effect is selected as a model SCOF, while ethanol (EtOH), benzene, and ammonia are set as model analytes. The fluorescence response of single-particle SCOF-301 (SSCOF-301) to these analytes is tracked in situ and in real time by monitoring the fluorescent signal on a laser scanning confocal microscope (LSCM), so that the individual fluorescence response of SCOF-301 is statistically analyzed. Furthermore, the proposed individual response mechanism allows providing theoretical guidance for the design of a functional COF sensor with suitable size and mechanism for different structural analytes.

METHODS

Synthesis of SCOF-301. SCOF-301 was synthesized by an amphiphilic amino acid aqueous strategy.[26] Typically, the amino acid derivative, palmitoylglycine (C16-GlyA, 3.1 g, Supporting Information), and NaOH (10 mmol) were first dissolved and stirred in water (10 mL) at 50 °C for 10 min. Then, 2,5-dihydroxyterephthalaldehyde (DHTA, 0.83 g) and 5 mL of tetrakis(4-aminophenyl)methane (TAM, 6 mol L^{-1}, *p*-toluenesulfonic acid as a solvent) were added, and the mixture was stirred for 10 min. Finally, the obtained products were collected by centrifugation and washed three times with water and tetrahydrofuran (THF). After immersing in THF for another 24 h, the products were further dried to obtain SCOF-301 powder with a length of about 10 μm. SCOF-301 with different sizes was obtained by controlling the concentration of monomers and C16-GlyA.

In Situ Fluorescence Monitoring. An in situ fluorescence monitoring system consisting of a confocal dish and LSCM was applied to monitor the response of SSCOF-301 to EtOH. The SCOF-301-dispersed aqueous solution (0.1 mg mL^{-1}, 1 μL) was dropped onto a confocal dish, prefrozen at −4 °C, and then put into a freeze-dryer for 48 h to remove moisture to obtain monodisperse SSCOF-301. After being fixed on the loading platform of the microscope system, the confocal dish was filled with EtOH via manual syringes of liquid chromatography. The certain concentration of EtOH vapor would be obtained after volatilization of the injected EtOH. Then, the LSCM was applied to record the images at a fixed *Z*-axis depth with excitation of light at 488 nm. Finally, ImageJ was used to obtain the pixel fluorescence intensity (F) and area (A, μm^2) of SSCOF-301. The concentration of EtOH vapor (c, mol L^{-1}) was calculated by the following formula[32]

$$c = \frac{\rho v_1 \times 10^{-3}}{M v_2}$$

where ρ (g cm^{-3}), v_1 (μL), and M (g mol^{-1}) are the density, volume, and molar mass of EtOH, respectively. v_2 is the volume of the sealing dish.

Fluorescence Change Ratio and Area Change Ratio. Pixel fluorescence change ratio (ΔFL) was used as an index to evaluate the fluorescence response of SSCOF-301 to EtOH and calculated by the following formula

$$\Delta \mathrm{FL} = \frac{F - F_0}{F_0}$$

Similarly, the area change ratio (ΔA) was used to describe the degree of deformation of SSCOF-301 after interaction with EtOH and calculated by the following formula

$$\Delta A = \frac{A - A_0}{A_0}$$

where F_0 and F are the pixel fluorescence intensity of SSCOF-301 before and after interaction with EtOH, respectively. A_0 and A are areas of SSCOF-301 before and after interaction with EtOH, respectively.

RESULTS AND DISCUSSION

In Situ Fluorescence Response of SSCOF-301 to EtOH. To investigate the fluorescence response of single-particle SCOF-301, the monodisperse micron-scale SCOF-301 with different sizes was prepared (Figures S1−S6).[26] The solid-state SCOF-301 gave double emission peaks at 588 and 737 nm under excitation of light at 488 nm (Figures S7 and S8), resulting from the ESIPT.[33] In contrast, COF-300 with the same structure of COF-301 but no OH group was prepared and exhibited only one emission peak, further proving the ESIPT of SCOF-301 (Figures S9 and S10). EtOH containing numerous H-bond acceptors to interfere

https://doi.org/10.1021/acs.analchem.4c00217
Anal. Chem. XXXX, XXX, XXX−XXX

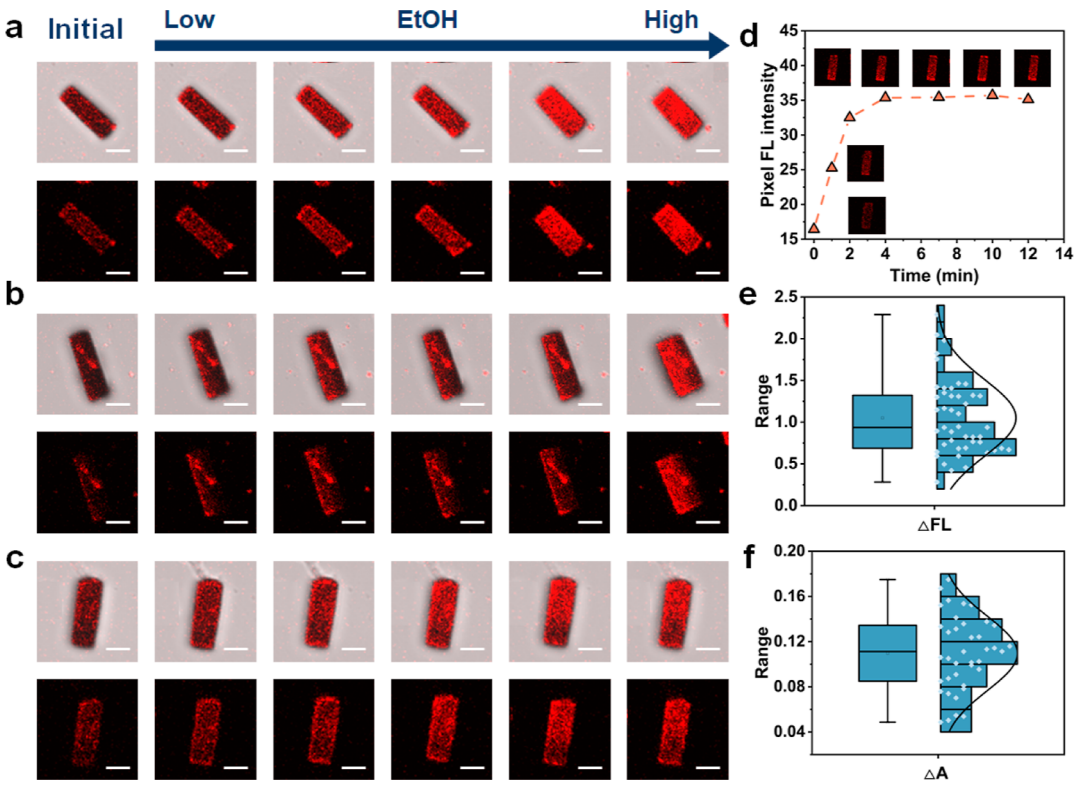

Figure 2. In situ LSCM images of SSCOF-301 with various crystal sizes after interaction with different concentrations of EtOH vapor: (a) 15.8 μm^2, (b) 19.9 μm^2, and (c) 21.3 μm^2 (scale bar: 3 μm.) (d) In situ fluorescence intensity of SSCOF-301 interacted with EtOH vapor at different times. Distribution maps of ΔFL (e) and Δ*A* (f) for SSCOF-301 with different crystal sizes, R^2 were 0.76 and 0.93, respectively.

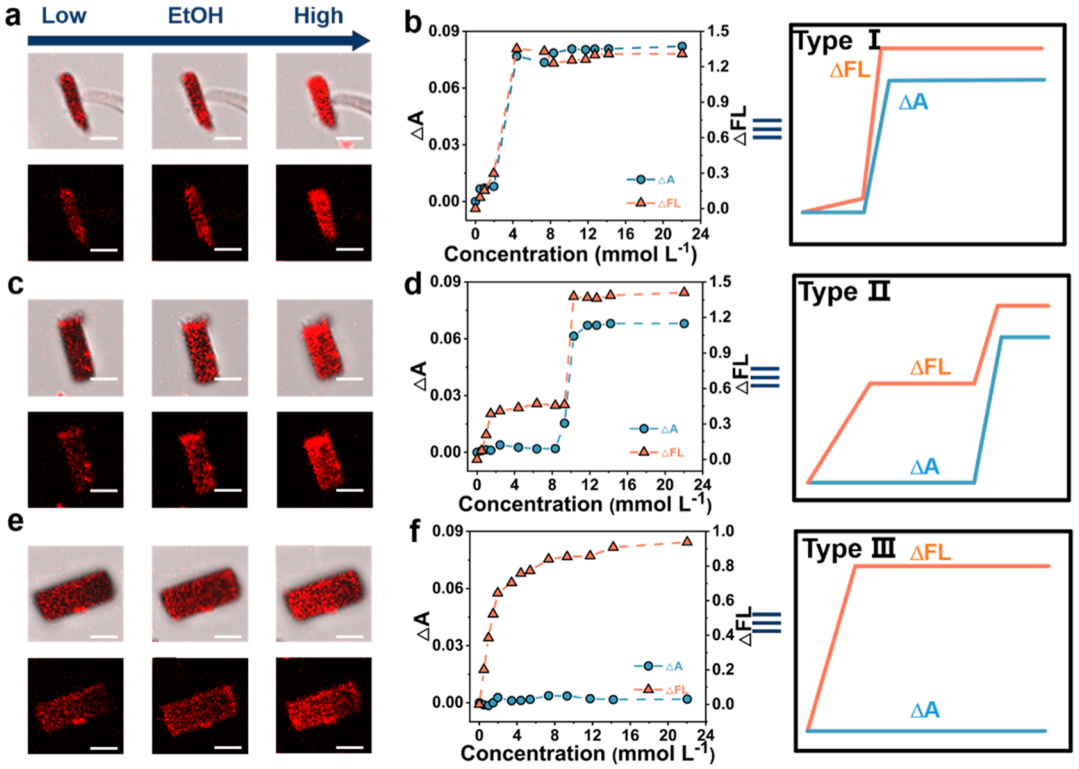

Figure 3. In situ LSCM images of SSCOF-301 with (a) type I, (c) type II, and (e) type III response to EtOH vapor (scale bar: 3 μm). Relationship of ΔFL/Δ*A* of SSCOF-301 and EtOH vapor in (b) type I, (d) type II, and (f) type III response.

with the intramolecular H-bond of SCOF-301 was selected as a model analyte. After interaction with EtOH, the fluorescence intensity of SCOF-301 at 588 nm enhanced, while the fluorescence at 737 nm decreased (Figure S8), indicating the

https://doi.org/10.1021/acs.analchem.4c00217
Anal. Chem. XXXX, XXX, XXX−XXX

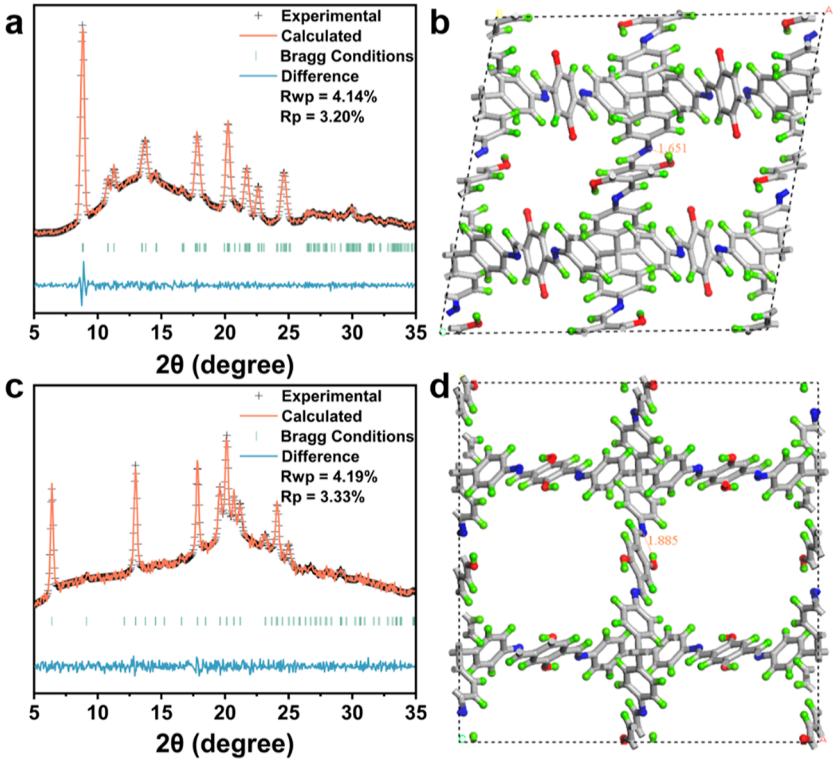

Figure 4. Pawley refined PXRD patterns of SCOF-301 before (a) and after (c) interaction with EtOH. Refined cell structure of SCOF-301 before (b) and after (d) interaction with EtOH (C, gray; N, blue; O, red; and H, green).

availability of tunable fluorescence emission of SCOF-301 with EtOH. Then, an in situ fluorescence recording system consisting of a confocal dish and LSCM was constructed (Figures 1 and S11). The confocal dish was applied to fix SSCOF-301 on the loading platform of the microscope system. A certain concentration of EtOH vapor in a confocal dish was obtained by injection of EtOH with manual syringe of liquid chromatography. The LSCM was utilized to record the fluorescence images of SSCOF-301 (500−600 nm) at a fixed *Z*-axis depth with excitation of light at 488 nm. Finally, ImageJ was used to obtain *F* and *A* of SSCOF-301.

The proposed fluorescence recording system allows in situ and real-time monitoring of the response of SSCOF-301 to EtOH. The pixel FL intensity of SSCOF-301 exhibited no obvious change in 15 days, indicating the stability of the COF and recording system (Figure S12). According to the in situ LSCM images of SSCOF-301, the pixel fluorescence of original SSCOF-301 first exhibited weak fluorescence, then started to enhance after the introduction of EtOH vapor, and finally tended to stabilize in about 4 min (Figure 2a−d). Moreover, SSCOF-301 with different crystal sizes gave individually different changes in shape besides the fluorescence after introduction of EtOH vapor (Figure S13).

ΔFL and Δ*A* were applied to illustrate the fluorescence and deformation response of SSCOF-301 to EtOH, respectively. The wide distribution of ΔFL (0.28−2.29) and Δ*A* (0.07−0.18) further confirmed that SSCOF-301 with different crystal sizes gave not only evident discrepancy in fluorescence change but also diverse deformation after interaction with EtOH (Figure 2e,f). Powder X-ray diffraction (PXRD) peaks of SCOF-301 shifted obviously after interaction with EtOH vapor, proving the structure change of SCOF-301 (Figure S14). No obvious change in Fourier transform infrared (FTIR) spectra and morphology of SCOF-301 after interaction with EtOH indicates that the fluorescence enhancement does not result from the structural disruption or collapse (Figures S15 and S16).

The effect of crystal sizes on response of SSCOF-301 to EtOH was investigated via analysis of the ΔFL and Δ*A* of SSCOF-301 with different crystal sizes under various concentrations of EtOH. Interestingly, the ΔFL and Δ*A* of SSCOF-301 after interaction with EtOH can be evidently divided into three categories named as type I, II, and III. In type I, a significant fluorescence enhancement of SSCOF-301 appeared during the deformation, and the fluorescence change was almost negligible before or after deformation (Figures 3a,b and S17a and b). In type II, the fluorescence evidently changed before and during deformation (Figures 3c,d and S17c,d). In type III, the fluorescence was significantly enhanced, and no obvious deformation was observed (Figures 3e,f and S17e,f). The statistical results further imply that the three response types of SSCOF-301 to EtOH are greatly related to crystal sizes (Figure S18). The small SSCOF-301 with areas of 6.3−12.6 μm^2 mainly trended to give type I response. The areas of SSCOF-301 corresponding to the type II response were mainly distributed from 13.4 to 19.9 μm^2. The large SSCOF-301 with 21.2−26.7 μm^2 would like to achieve a type III response.

In Situ Fluorescence Response of SSCOF-301 to Benzene and Ammonia. In contrast to EtOH, benzene was selected as another analyte because benzene can hardly provide a H-bond acceptor to compete the intramolecular H-bond site of SSCOF-301 but can bring the deformation of SSCOF-301. The evident fluorescence enhancement at 588 nm and shifted PXRD diffraction peaks of SSCOF-301 confirmed the fluorescence change and deformation of SSCOF-301 caused by benzene (Figures S19 and S20). In

https://doi.org/10.1021/acs.analchem.4c00217
Anal. Chem. XXXX, XXX, XXX−XXX

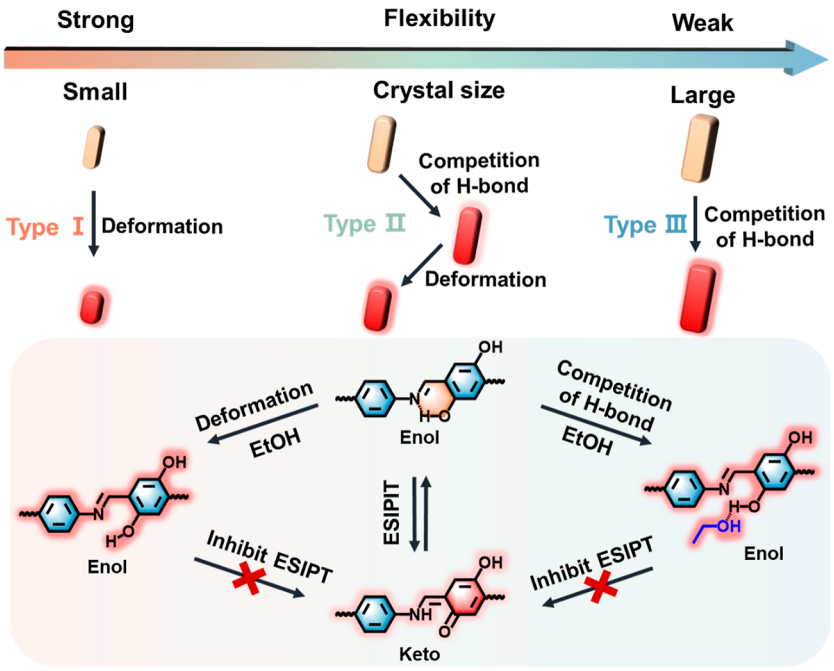

Figure 5. Response mechanism of SSCOF-301 to EtOH related to the crystal sizes.

addition, all of the SSCOF-301 with different sizes only gave the typical type I response to benzene (Figure S21).

Ammonia was selected as another analyte because ammonia exhibits the analogous H-bond acceptor with EtOH but cannot bring deformation of SSCOF-301 due to the molecular size and aggregation form in the COF pore.[19,26] No obvious PXRD peak change confirmed no deformation of SSCOF-301 after interaction with ammonia (Figures S22 and S23). The response of all of SSCOF-301 with different sizes to ammonia was classified in type III (Figure S24).

Crystal Size-Dependent Fluorescence Response Mechanism. The reason why the fluorescence of SSCOF-301 changed after interaction with the model analytes of EtOH was first figured out. As we know, the intramolecular H-bond renders SSCOF-301 with an evident ESIPT effect. The protons can availably transfer from −OH to −C═N under photoexcitation, resulting in transformation of enol structure (emission at 588 nm) to keto structure (emission at 737 nm) (Figure S25). When EtOH was introduced, on the one hand, EtOH can inhibit the ESIPT effect through competition of the H-bond site of SCOF-301. On the other hand, 3D COFs prepared with the monomer of TAM were well known for their dynamical structure.[34,35] Thus, the entrance of EtOH would cause the deformation of SCOF-301. Pawley refinement with experimental PXRD showed that the distance of N and H in SCOF-301 increased from 1.673 to 1.885 Å after interaction with EtOH. The increasing distance of intramolecular H-bond makes the overlap area of the electron decrease (Figure 4 and Tables S1−S4), which would also weaken the ESIPT effect. In short, both the competition of the H-bond site and deformation can decrease the ESIPT effect of SSCOF-301 (Figure 5) and then induce the fluorescence changes. Accordingly, the fluorescence changes of SSCOF-301 to benzene only attributed to the deformation due to no existence of competition of the H-bond site, while the response of SSCOF-301 ammonia is caused by the competition of the H-bond site because of no appearance of deformation.

The mechanism for three different deformation and competition H-bond site-induced responses of SSCOF-301 to EtOH related to crystal size also needed to be illustrated. SSCOF-301 with different sizes gave the typical type I response to benzene, indicating the dominant deformation for the type I response, while the response of all SSCOF-301 with different sizes to ammonia was classified in type III, proving the dominant role of competition of the H-bond site in this type of response. Furthermore, benzene can bring the fluorescence change of small-sized SCOF-301 (6.3−12.6 μm^2) at a concentration of 2.4 mmol L^{-1}, evidently lower than that of ammonia (7.6 mmol L^{-1}), demonstrating that deformation is more sensitive than competition of the H-bond site for fluorescence change in small-sized SSCOF-301 (Figures S18, S26, and S27). The small-sized crystal of SSCOF-301 gives a more flexible structure to deform, thereby it is easier to exhibit the type I response to EtOH dominated by the deformation (Figure 5). The comparable concentration of benzene (8.0 mmol L^{-1}) and ammonia (7.6 mmol L^{-1}) triggered that the fluorescence change of medium-sized SSCOF-301 (13.4−19.9 μm^2) indicates a similar sensitivity of competition of the H-bond site and deformation for the fluorescence change of SSCOF-301 in this size range (Figures S28 and S29). The increase of the crystal size makes the medium-sized SSCOF-301 become rigid and difficult to deformation, and then the competition of the H-bond site was evidently involved for fluorescence change. So, the medium-sized SSCOF-301 tended to give type II response resulted from both competition of the H-bond site and deformation (Figure 5). The lower concentration triggered that the fluorescence enhancement of ammonia (7.6 mmol L^{-1}) than that of benzene (18.5 and 13.7 mmol L^{-1}) for large-sized SSCOF-301 (21.2−26.7 μm^2) confirmed more sensitivity of competition of the H-bond site than deformation in control of the fluorescence change (Figures S30 and S31). Different from benzene, EtOH can hardly make the large-sized SSCOF-301 deform, leading to the type III response dominantly controlled with competition of the H-bond site of SSCOF-301 to EtOH.

https://doi.org/10.1021/acs.analchem.4c00217
Anal. Chem. XXXX, XXX, XXX−XXX

Guidance for Sensing. The three different size-dependent response mechanisms of SSCOF-301 to EtOH indicate that SSCOF-301 with different sizes and response mechanisms gives a significant effect on the sensitivity of sensing. Thus, slope (k) of the calibration curve for EtOH sensing based on SSCOF-301 with different crystal sizes was further studied. Generally, the small-sized SSCOF-301 gave higher k values than large-sized SSCOF-301. The fitting normal distribution showed that the largest k was achieved with the SSCOF-301 at size of about 9.6 μm^2 (Figure S32). Furthermore, the distribution of k along the three different response types of SSCOF-301 to EtOH exhibited that SSCOF-301 with type I response triggered by deformation gave maximum k values (Figure S33), indicating that the deformation is more sensitive than the competition of the H-bond site or their combination for sensing. As we discussed before, the smaller crystal of SSCOF-301 with more flexible structure is more accessible to deformation and thus is more conducive to the development of effective sensors.

CONCLUSIONS

In summary, we have achieved fluorescence response of a single-particle SCOF and further revealed a size-dependent deformation and competition H-bond site-induced response mechanism of SCOF. Both deformation and competition of the H-bond site were found to be responsible for the fluorescence change of the proposed SCOF through in situ monitoring of the fluorescent signal. In addition, the increase of crystal size caused the dominant role for fluorescence change to vary from deformation to competition of the H-bond site, which gave three different response types of SCOF to the analytes. We believe that the proposed size-dependent deformation and competition H-bond site-induced fluorescence response mechanism can effectively guide the design of functional COF sensors with suitable size and mechanism for different structural analytes.

ASSOCIATED CONTENT

Supporting Information

The Supporting Information is available free of charge at https://pubs.acs.org/doi/10.1021/acs.analchem.4c00217.

Additional data including chemicals and materials, characterization, and experimental details (PDF)

AUTHOR INFORMATION

Corresponding Author

Hai-Long Qian − *State Key Laboratory of Food Science and Resources, Jiangnan University, Wuxi 214122, China; Institute of Analytical Food Safety, School of Food Science and Technology, Jiangnan University, Wuxi 214122, China;* orcid.org/0000-0001-7554-4115; Email: hlqian@jiangnan.edu.cn

Authors

Yan Wang − *Institute of Analytical Food Safety, School of Food Science and Technology, Jiangnan University, Wuxi 214122, China*

Xu-Qin Ran − *Institute of Analytical Food Safety, School of Food Science and Technology, Jiangnan University, Wuxi 214122, China*

Cheng Yang − *State Key Laboratory of Food Science and Resources, Jiangnan University, Wuxi 214122, China; Institute of Analytical Food Safety, School of Food Science and Technology, Jiangnan University, Wuxi 214122, China*

Xiu-Ping Yan − *State Key Laboratory of Food Science and Resources, Jiangnan University, Wuxi 214122, China; Institute of Analytical Food Safety, School of Food Science and Technology and Key Laboratory of Synthetic and Biological Colloids, Ministry of Education, School of Chemical and Material Engineering, Jiangnan University, Wuxi 214122, China;* orcid.org/0000-0001-9953-7681

Complete contact information is available at: https://pubs.acs.org/10.1021/acs.analchem.4c00217

Notes

The authors declare no competing financial interest.

ACKNOWLEDGMENTS

This work was supported by the National Natural Science Foundation of China (nos. 22376082, 22076066, and 22176073), the Jiangsu Funding Program for Excellent Postdoctoral Talent (no. 2023ZB116), the Youth Program of Nature Science Foundation of Shandong Province, and the "Fundamental Research Funds for the Central Universities". The author thanks the help from Pro. Zhikun Zheng, Sun Yat-sen University, in preparation and characterization of single-crystal COF-301.

REFERENCES

(1) Côté, A. P.; Benin, A. I.; Ockwig, N. W.; O'Keeffe, M.; Matzger, A. J.; Yaghi, O. M. *Science* **2005**, *310*, 1166−1170.

(2) Waller, P. J.; Gandara, F.; Yaghi, O. M. *Acc. Chem. Res.* **2015**, *48*, 3053−3063.

(3) Skorjanc, T.; Shetty, D.; Valant, M. *ACS Sens.* **2021**, *6*, 1461−1481.

(4) Haug, W. K.; Moscarello, E. M.; Wolfson, E. R.; McGrier, P. L. *Chem. Soc. Rev.* **2020**, *49*, 839−864.

(5) Liu, X.; Huang, D.; Lai, C.; Zeng, G.; Qin, L.; Wang, H.; Yi, H.; Li, B.; Liu, S.; Zhang, M.; Deng, R.; Fu, Y.; Li, L.; Xue, W.; Chen, S. *Chem. Soc. Rev.* **2019**, *48*, 5266−5302.

(6) Ahmed, I.; Jhung, S. H. *Coord. Chem. Rev.* **2021**, *441*, 213989.

(7) Xue, R.; Guo, H.; Wang, T.; Gong, L.; Wang, Y.; Ai, J.; Huang, D.; Chen, H.; Yang, W. *Anal. Methods* **2017**, *9*, 3737−3750.

(8) Das, P.; Chakraborty, G.; Mandal, S. K. *ACS Appl. Mater. Interfaces* **2020**, *12*, 10224−10232.

(9) Zhang, C.; Zhang, S.; Yan, Y.; Xia, F.; Huang, A.; Xian, Y. *ACS Appl. Mater. Interfaces* **2017**, *9*, 13415−13421.

(10) Ding, S. Y.; Dong, M.; Wang, Y. W.; Chen, Y. T.; Wang, H. Z.; Su, C. Y.; Wang, W. *J. Am. Chem. Soc.* **2016**, *138*, 3031−3037.

(11) Wang, P.; Zhou, F.; Zhang, C.; Yin, S. Y.; Teng, L.; Chen, L.; Hu, X. X.; Liu, H. W.; Yin, X.; Zhang, X. B. *Chem. Sci.* **2018**, *9*, 8402−8408.

(12) Liu, Y.; Yan, X.; Lu, H.-S.; Zhang, W.-D.; Shi, Y.-X.; Gu, Z.-G. *Sens. Actuators, B* **2020**, *323*, 128708.

(13) Feng, X.; Ding, X.; Jiang, D. *Chem. Soc. Rev.* **2012**, *41*, 6010−6022.

(14) Navarro, J. A. R. *Science* **2018**, *361*, 35.

(15) Zhu, Y. L.; Zhao, H. Y.; Fu, C. L.; Li, Z. W.; Sun, Z. Y.; Lu, Z. *J. Phys. Chem. Lett.* **2020**, *11*, 9952−9956.

(16) Castano, I.; Evans, A. M.; Li, H.; Vitaku, E.; Strauss, M. J.; Bredas, J. L.; Gianneschi, N. C.; Dichtel, W. R. *ACS Cent. Sci.* **2019**, *5*, 1892−1899.

(17) Wang, S.; Reddy, V. A.; Ang, M. C.; Cui, J.; Khong, D. T.; Han, Y.; Loh, S. I.; Cheerlavancha, R.; Singh, G. P.; Rajani, S.; Strano, M. S. *J. Am. Chem. Soc.* **2023**, *145*, 12155−12163.

(18) Kang, C.; Zhang, Z.; Usadi, A. K.; Calabro, D. C.; Baugh, L. S.; Yu, K.; Wang, Y.; Zhao, D. *J. Am. Chem. Soc.* **2022**, *144*, 3192−3199.

(19) Ma, T.; Kapustin, E. A.; Yin, S. X.; Liang, L.; Zhou, Z.; Niu, J.; Li, L.-H.; Wang, Y.; Su, J.; Li, J.; Wang, X.; Wang, W. D.; Wang, W.; Sun, J.; Yaghi, O. M. *Science* **2018**, *361*, 48−52.
(20) Guo, Z.; Li, G.; Wang, H.; Zhao, J.; Liu, Y.; Tan, H.; Li, X.; Stang, P. J.; Yan, X. *J. Am. Chem. Soc.* **2021**, *143*, 9215−9221.
(21) Lin, Y.; Yu, L.; Wang, H.; Li, J. *CrystEngComm* **2020**, *22*, 5946−5948.
(22) Yamaji, M.; Kato, S. I.; Tomonari, K.; Mamiya, M.; Goto, K.; Okamoto, H.; Nakamura, Y.; Tani, F. *Inorg. Chem.* **2017**, *56*, 12514−12519.
(23) Evans, A. M.; Parent, L. R.; Flanders, N. C.; Bisbey, R. P.; Vitaku, E.; Kirschner, M. S.; Schaller, R. D.; Chen, L. X.; Gianneschi, N. C.; Dichtel, W. R. *Science* **2018**, *361*, 52−57.
(24) Liang, L.; Qiu, Y.; Wang, W. D.; Han, J.; Luo, Y.; Yu, W.; Yin, G. L.; Wang, Z. P.; Zhang, L.; Ni, J.; Niu, J.; Sun, J.; Ma, T.; Wang, W. *Angew. Chem., Int. Ed.* **2020**, *59*, 17991−17995.
(25) Wang, X.; Enomoto, R.; Murakami, Y. *Chem. Commun.* **2021**, *57*, 6656−6659.
(26) Zhou, Z.; Zhang, L.; Yang, Y.; Vitorica-Yrezabal, I. J.; Wang, H.; Tan, F.; Gong, L.; Li, Y.; Chen, P.; Dong, X.; Liang, Z.; Yang, J.; Wang, C.; Hong, Y.; Qiu, Y.; Golzhauser, A.; Chen, X.; Qi, H.; Yang, S.; Liu, W.; Sun, J.; Zheng, Z. *Nat. Chem.* **2023**, *15*, 841−847.
(27) Zhang, G.; Zou, X.; Wang, Q.; He, Y. *Angew. Chem., Int. Ed.* **2023**, *62*, No. e202214569.
(28) Chi, H.; Liu, Y.; Li, Z.; Chen, W.; He, Y. *Nat. Commun.* **2023**, *14*, 5061.
(29) Zheng, Q.; Huang, J.; He, Y.; Huang, H.; Ji, Y.; Zhang, Y.; Lin, Z. *ACS Appl. Mater. Interfaces* **2022**, *14*, 9754−9762.
(30) Ma, T.; Wei, L.; Liang, L.; Yin, S.; Xu, L.; Niu, J.; Xue, H.; Wang, X.; Sun, J.; Zhang, Y. B.; Wang, W. *Nat. Commun.* **2020**, *11*, 6128.
(31) Tan, F.; Han, S.; Peng, D.; Wang, H.; Yang, J.; Zhao, P.; Ye, X.; Dong, X.; Zheng, Y.; Zheng, N.; Gong, L.; Liang, C.; Frese, N.; Golzhauser, A.; Qi, H.; Chen, S.; Liu, W.; Zheng, Z. *J. Am. Chem. Soc.* **2021**, *143*, 3927−3933.
(32) El-Mahdy, A. F. M.; Lai, M. Y.; Kuo, S. W. *J. Mater. Chem. C* **2020**, *8*, 9520−9528.
(33) Zhou, P.; Han, K. *Acc. Chem. Res.* **2018**, *51*, 1681−1690.
(34) Wei, L.; Sun, T.; Shi, Z.; Xu, Z.; Wen, W.; Jiang, S.; Zhao, Y.; Ma, Y.; Zhang, Y. B. *Nat. Commun.* **2022**, *13*, 7936.
(35) Chen, Y.; Shi, Z. L.; Wei, L.; Zhou, B.; Tan, J.; Zhou, H. L.; Zhang, Y. B. *J. Am. Chem. Soc.* **2019**, *141*, 3298−3303.

https://doi.org/10.1021/acs.analchem.4c00217
Anal. Chem. XXXX, XXX, XXX−XXX